

Multiband Superconductivity in $\text{Lu}_3\text{Os}_4\text{Ge}_{13}$

Om Prakash* and A. Thamizhavel, S. Ramakrishnan
*Department of Condensed Matter Physics and Materials Science,
Tata Institute of Fundamental Research, Mumbai-400005, India*

Intermetallic $\text{R}_3\text{T}_4\text{X}_{13}$ series consists of cage like structure and have been in focus due to their unconventional electronic ground states. In this work, we report the normal and superconducting state properties of a high quality single crystal of $\text{Lu}_3\text{Os}_4\text{Ge}_{13}$. $\text{Lu}_3\text{Os}_4\text{Ge}_{13}$ belongs to the above mentioned series and crystallizes in a cubic crystal structure with the space group $Pm\bar{3}n$. Using electrical transport, magnetization and heat capacity measurements, we show that $\text{Lu}_3\text{Os}_4\text{Ge}_{13}$ is a type-II multi-band superconductor ($T_c = 3.1$ K) with unusual superconducting properties. The analysis of the low temperature heat capacity data suggests that $\text{Lu}_3\text{Os}_4\text{Ge}_{13}$ is a moderately coupled multi-band BCS superconductor with two gaps ($2\Delta/k_B T_c = 3.68 \pm 0.04$ & 0.34 ± 0.02) in the superconducting state. The dc-magnetization ($M - H$) shows a large reversible region in the superconducting state similar to the vortex liquid phase observed in high- T_c superconductors. The value of the Ginzburg number G_i suggests that the thermal fluctuations, though small as compared to those in high- T_c cuprates, may play an important role in the unpinning of the vortices in this compound. The electronic band structure calculations show that three bands cross the Fermi level and constitute a complex Fermi surface in $\text{Lu}_3\text{Os}_4\text{Ge}_{13}$.

I. INTRODUCTION

Ternary intermetallic compounds with the formula $R_3T_4X_{13}$, where R is a rare-earth element, T transition metal and X semi-metallic/semiconducting element, have significantly contributed to the understanding of the physics of strongly correlated materials. These compounds show a variety of unusual magnetic ground states and superconductivity at low temperatures¹. One such structure with no metalloids was reported by Remeika *et al*². These compounds ($R_3T_4X_{13}$) crystallize in a cubic structure (space group $Pm\bar{3}n$) and feature cage-like environment within the unit cell. Amongst these, La, Yb, and Th based compounds are superconducting, whereas, Gd and Eu based compounds show magnetic transition. By replacing Sn by Ge and Rh by Ru in $R_3Rh_4Sn_{13}$, Segre and Braun³ reported superconductivity and magnetic ordering. Our studies on polycrystalline samples of $R_3Ru_4Ge_{13}$ series (R=Y, Ce, Pr, Nd, Ho, Er, Dy, Yb, Lu) showed⁴⁻⁶ that the series exhibit unusual physical properties. These properties could be considered as those belonging to the semi-metals or low band-gap semiconductors. Studies on Lu and Ru based polycrystalline samples⁶ reported superconductivity below 2.3 K and 2.8 K respectively. These compounds are also reported as good thermoelectric materials⁷. The multi-valley nature of the band structure⁸, cage like coordination in the crystal structure and occurrence of superconductivity make iso-structural $Lu_3Os_4Ge_{13}$ an interesting compound to look for unusual superconductivity. Bulk studies show that $Lu_3Os_4Ge_{13}$ is a multi-band superconductor and it shows a large reversible region in the magnetization (M-H) data, which has been usually observed in high T_c superconductors¹⁰. In this report, we present detailed study of the anomalous superconducting properties of $Lu_3Os_4Ge_{13}$ single crystal, supported by the electronic band structure calculations.

II. METHODS

A. Sample preparation and characterization

The single crystal of $Lu_3Os_4Ge_{13}$ was grown using the Czochralski crystal pulling method in a tetra-arc furnace under inert Argon atmosphere. Stoichiometric mixture (10 g) of highly pure elements (Lu: 99.99%, Os: 99.99%, Ge: 99.99%) was melted 4-5 times in the same furnace to make a homogeneous polycrystalline sample. The single crystal was pulled from the polycrystalline melt using a tungsten seed rod at the rate of 10 mm/h for about 6 hrs to get 5 – 6 cm long cylindrical shaped crystals with 3 – 4 mm diameter. $Lu_3Os_4Ge_{13}$ crystallizes in cubic crystal structure with space group $Pm\bar{3}n$ (space group number 223) with 40 atoms per unit cell (2 formula unit). The structure is similar to that of iso-structural compound $Y_3Ru_4Ge_{13}$ ¹⁸. The unit cell contains two inequivalent Ge sites. One can visualize $Lu_3Os_4Ge_{13}$ structure as a unit consisting of three substructures: edge-sharing Ge1(Ge2)12 icosahedra, Lu-centered cubotahedra R(Ge2)12, and corner-sharing Os(Ge2)6 trigonal prisms. The corner-sharing Os(Ge2)6 trigonal prisms create “cages” containing a Ge1 atom similar to the cages observed in Skutterudites³⁰. The crystal structure of $Lu_3Os_4Ge_{13}$ is shown in Fig. 1. The room temperature powder XRD data were analyzed by structural Rietveld refinement¹⁹ using the Fullprof program (shown in Fig. 1) and the refinement confirmed single phase nature of the sample. The global $\chi^2 = 2.74$ is obtained from the refinement. The values of lattice constants obtained from the refinement are $a = b = c = 8.94585 (\pm 0.00022 \text{ \AA})$. The crystal was characterized using various experimental

TABLE I. Crystal structure parameters obtained from the Rietveld refinement of the room temperature powder x-ray diffraction data of $Lu_3Os_4Ge_{13}$. Profile reliability factor $R_p = 17.5\%$, weighted profile R -factor $R_{wp} = 17.2\%$, Bragg R -factor = 8.46% and R_f -factor = 7.44% were obtained from the best fit.

Structure	Cubic			
Space group	$Pm\bar{3}n$ (No. 223)			
Lattice parameters				
a (Å)	8.94585(22)			
V_{cell} (Å ³)	715.921(0.030)			
Atomic coordinates				
Atom	Wyckoff position	x	y	z
Lu	6c	0.25	0	0.50
Os	8e	0.25	0.25	0.25
Ge1	24k	0	0.31206(30)	0.14965(32)
Ge2	2a	0	0	0

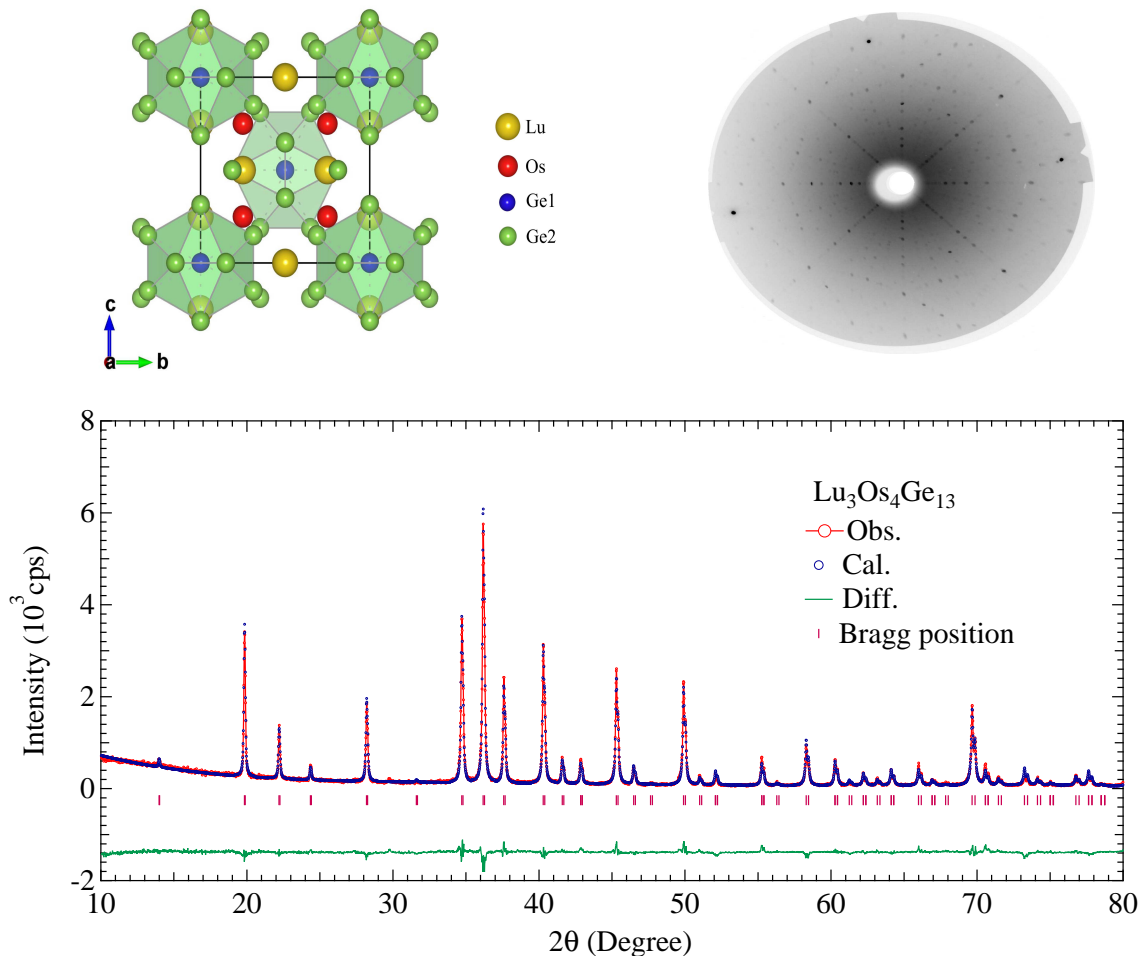


FIG. 1. (Color online) 1. Top left panel: Crystal structure of $\text{Lu}_3\text{Os}_4\text{Ge}_{13}$ projected along (100) plane. 2. Top right panel: Laue diffraction pattern for (100) plane of $\text{Lu}_3\text{Os}_4\text{Ge}_{13}$. 3. Bottom panel: Rietveld fit of the powder XRD data of $\text{Lu}_3\text{Os}_4\text{Ge}_{13}$. The unit cell consists of cage like crystal structure as shown in the left panel. The Rietveld analysis and circular spots in the Laue diffraction confirm the high quality, single phase and single-crystalline nature of the grown crystal.

techniques such as room temperature powder X-ray diffraction (PXRD), electron probe micro-analyzer (EPMA) and energy dispersive X-ray spectroscopy (EDX) and confirmed to be a well defined single crystal with no trace of impurity phases. The EPMA and EDX characterizations were done on the well polished surfaces and confirmed the proper stoichiometry (3 : 4 : 13) and single phase nature of $\text{Lu}_3\text{Os}_4\text{Ge}_{13}$ compound. The single crystals were oriented along the crystallographic direction [100] using Laue back reflection method using the Huber Laue diffractometer and cut to the desired shape and dimensions using a spark erosion cutting machine.

B. Measurement techniques

The electrical resistivity was measured using standard four-probe technique in a home made setup. $40\ \mu\text{m}$ diameter Au wires were used for making electrical connections using indium solder. The contact resistance is of the order of $10\text{m}\Omega$. The zero magnetic field data was recorded in the temperature range 1.6-300 K using LR700 resistance bridge. The electrical resistivity was measured in constant magnetic fields (0-5.5 T) in a Cambridge Magnetic Refrigeration (CMR) mFridge refrigerator setup from 0.1-4.2 K for determining the upper critical field $\mu_0 H_{c2}(T)$. The CMR setup can reach to base temperature of $\approx 100\text{mK}$ using adiabatic demagnetization of paramagnetic salt pills. Magnetic susceptibility was measured using a commercial superconducting quantum interferometer device (SQUID) magnetometer (MPMS5, Quantum Design, USA) in a constant magnetic field of 10 mT; the sample was cooled down to 1.8 K in zero-magnetic field and then the magnetic field was applied, followed by warming to 5 K (this is called the zero field

cooled "ZFC" data). Then the sample was cooled down to 1.8 K in the magnetic field of 10 mT to take field cooled (FC) data. The heat capacity was measured using Physical Property Measurement System (PPMS), equipped with He³ dilution refrigerator in the temperature range 0.05-4 K and 1.8-300K by a time-relaxation method in different magnetic fields from 0-7 T.

C. Band structure calculations

The electronic band structure calculations were performed by density functional theory (DFT) using WIEN2k code with a full-potential linearised augmented plane-wave and local orbitals (FP-LAPW + lo) basis,^{20,21} together with Perdew-Burke-Ernzerhof (PBE) parametrization²³ of the generalized gradient approximation (GGA), with no spin-orbit coupling. The plane wave cutoff parameter $R_{MT}K_{MAX} = 7$ was taken with 5000 k-points (the choice of number of k points varies with symmetry of crystal structure and lower symmetry structure may require larger number of k-point sampling). The program xCrysden was used for calculating and plotting bands and Fermi surface.

III. RESULTS AND DISCUSSION

Fig. 2(a) shows the electrical resistivity of Lu₃Os₄Ge₁₃ for current parallel to the [100]-direction measured in the temperature range from 2-300 K. A negative temperature coefficient of resistivity ($\frac{d\rho}{dT} < 0$) is observed in the normal state. This can result from several mechanisms such as site disorder, electronic correlations and low energy phonon scattering. The compound under study has a cage like structure with a loosely bound Ge atom within the cage, which gives rise to the low energy soft phonon modes resulting in significant electron-phonon scattering at low temperatures. The resistivity becomes zero at the onset of superconductivity below 3.1 K. Inset in Fig. 2(a) shows the change in the superconducting transition temperature in different magnetic fields. The width of the superconducting transition (ΔT) increases with increasing magnetic field. The transition temperature is taken at the point where the resistivity drops to 50% of the normal state value. Fig. 2(b) shows the temperature dependence of the upper critical field $\mu_0 H_{c2}$. A linear relationship is observed between H_{c2} and temperature in the proximity of the transition temperature (T_c at $H = 0$).

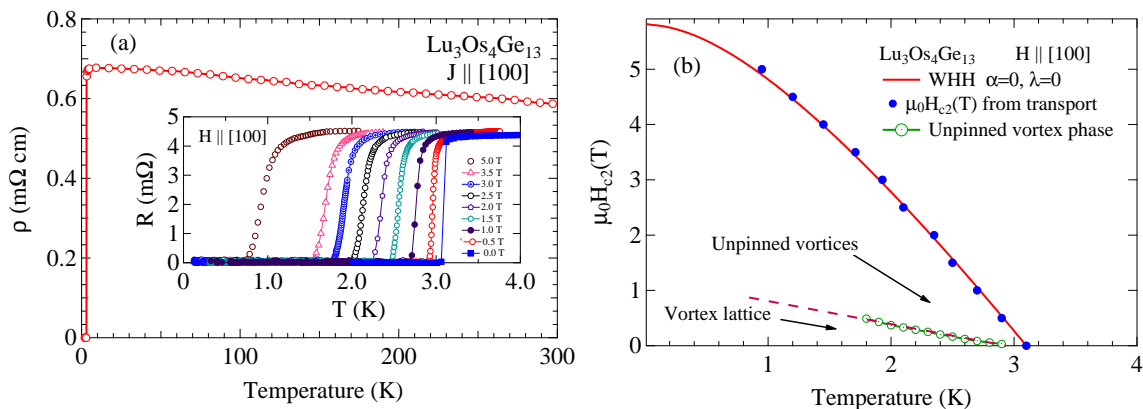


FIG. 2. (Color online) (a) Temperature dependence of the electrical resistivity (ρ) for the current parallel to the [100] direction of Lu₃Os₄Ge₁₃ from 2-300 K. The inset shows the effect of the magnetic field on the superconducting transition temperature. (b) Temperature dependence of the upper critical $\mu_0 H_{c2}$. The red curve correspond to the simulated WHH expression (6) in the dirty limit for $\alpha = 0$, $\lambda = 0$. The open green circles shows the phase boundary between the vortex lattice and unpinned vortex phase, as observed in the magnetization data.

In type-II superconductors, an external magnetic field leads to the Cooper pair breaking via two mechanisms, orbital and spin-paramagnetic effects^{9,26,28} (the latter also known as Pauli paramagnetic limiting effect). The orbital pair breaking is related to the emergence of Abrikosov vortices. The orbital limiting field refers to the magnetic field at which the vortex cores fill the whole volume and is given by the formula,

$$H_{c2}^{\text{orb}}(0) = \Phi_0 / 2\pi\xi^2, \quad (1)$$

where ξ is the Ginzburg-Landau coherence length and Φ_0 ($= hc/2e = 2.07 \times 10^{-15} \text{Tm}^2$), is the magnetic flux quantum. For the single band BCS superconductors, $H_{c2}^{\text{orb}}(0)$ is derived from the slope of the $H_{c2}(T)$ -T phase boundary at T_c , given by,

$$\mu_0 H_{c2}^{\text{orb}}(0) = -0.69 T_c \left. \frac{dH_{c2}}{dT} \right|_{T=T_c}, \quad (2)$$

in the dirty limit and

$$\mu_0 H_{c2}^{\text{orb}}(0) = -0.73 T_c \left. \frac{dH_{c2}}{dT} \right|_{T=T_c}, \quad (3)$$

in the clean limit of the Werthamer-Helfand-Hohenberg (WHH) theory¹¹.

The spin paramagnetic pair breaking mechanism is related to the Zeeman splitting of the spin singlet Cooper pairs due to the interaction of the magnetic field with electron spins. For a BCS superconductor, the Pauli limiting field is given by $H^{\text{Pauli}} = 1.82 T_c = 5.80 T$. The upper critical field $\mu_0 H_{c2}$ is influenced by both orbital and spin paramagnetic effects. Orbital pair breaking is the dominant mechanism at low magnetic fields and Pauli paramagnetic effect dominates the upper critical field at very high magnetic fields. The relative importance of the Orbital and Pauli limiting fields is described by the Maki parameter ' α '¹² defined as,

$$\alpha = \sqrt{2} H_{c2}^{\text{orb}}(0) / H^{\text{Pauli}}(0). \quad (4)$$

The value of the orbital critical field calculated using equation (2) is 5.45 T. The Ginzburg-Landau coherence length, $\xi(0)_{\text{GL}}$ is given by,

$$\xi(0)_{\text{GL}} = \sqrt{\Phi_0 / 2\pi H_{c2}^{\text{orb}}(0)}. \quad (5)$$

Using equation (5), we get $\xi(0)_{\text{GL}} = 78 \text{\AA}$. Using the values of $\mu_0 H_{c2}^{\text{orb}}(0)$ and $\mu_0 H^{\text{Pauli}}$, the value of the Maki parameter comes out to be $\alpha = 1.33$.

The temperature dependence of H_{c2} for single-band, dirty limit superconductors is given by the WHH formula,

$$\ln\left(\frac{1}{t}\right) = \sum_{\nu=-\infty}^{\nu=\infty} \left\{ \frac{1}{|2\nu+1|} - \left[|2\nu+1| + \frac{\bar{h}}{t} + \frac{(\alpha\bar{h}/t)^2}{|2\nu+1| + (\lambda_{so} + \bar{h})/t} \right]^{-1} \right\}, \quad (6)$$

where $t = T/T_c$, $\bar{h} = 4H_{c2}(T)/(\pi^2 T_c \left. \frac{dH_{c2}(T)}{dT} \right|_{T_c})$, α is the Maki parameter, and λ_{so} is the spin-orbit scattering constant. When $\lambda_{so} = 0$, $H_{c2}(0)$ obtained from WHH formula satisfies the relation,

$$H_{c2}(0) = H_{c2}^{\text{orb}}(0) / \sqrt{1 + \alpha^2}. \quad (7)$$

In Fig. 2(b), we note that the experimental H_{c2} vs T data is best described by the WHH formula for $\alpha = 0$ ($H_{c2}^{\text{orb}}(0) \ll H^{\text{Pauli}}(0)$), $\lambda_{so} = 0$ (red dashed curve). If we use $\alpha = 1.33$, as derived above, the WHH formula does not explain the data except when $\lambda_{so} \approx 100$, which is clearly unphysical. This suggests that single band models are not enough to describe the temperature dependence of upper critical field $H_{c2}(T)$ and multi-band effects have to be included in the models to describe the data. The multi-band models²⁷ need parameters like inter-band coupling constants and knowledge of Matsubara frequencies for the specific compound and these are not yet known for $\text{Lu}_3\text{Os}_4\text{Ge}_{13}$. Assuming moderate multi-band effects present in this compound, if we do a linear extrapolation of the $H_{c2}(T)$ at T=0 in Fig. 2(b), we get an estimate of the $H_{c2}(0) = 6.8T$, which is $\approx 1\text{T}$ more than the value obtained from WHH theory. With this observation, to an first order approximation, we can use single band models to get approximate values of superconducting state parameters, like coherence length, penetration depth etc.

Fig. 3(a) shows the zero field heat capacity data of $\text{Lu}_3\text{Os}_4\text{Ge}_{13}$ in the temperature range 1.8-300K. The experimental value of heat capacity $C(T = 300\text{K}) = 504 \text{ Jmole}^{-1}\text{K}^{-1}$ is very close to the Dulong-Petit high-temperature limit of the lattice heat capacity $C_v = 3NR = 498.9 \text{ Jmole}^{-1}\text{K}^{-1}$. The electronic contribution to the heat capacity $C_{el}(T)$ can be calculated by subtracting the phonon contribution from the total heat capacity $C(T)$, i.e. $C_{el}(T) = C(T) - \beta T^3$. Fig. 3(b) shows a sharp jump in the heat capacity at 3.1 K which confirms the bulk superconductivity in the compound. Fig. 3(e) shows the heat capacity data measured in different magnetic fields ($H \perp [100]$). The magnitudes of the heat capacity jump as well as T_c decrease with increasing magnetic field.

The superconductivity is fully suppressed in a magnetic field of 7 T and the data is fitted to the equation $C(T) = \gamma_n T + \beta T^3$ as shown in Fig. 3(b), where $\gamma_n T$ represents the electronic contribution and βT^3 describe the lattice-phonon contribution to the specific heat in the normal state. We find the electronic specific heat coefficient $\gamma_n =$

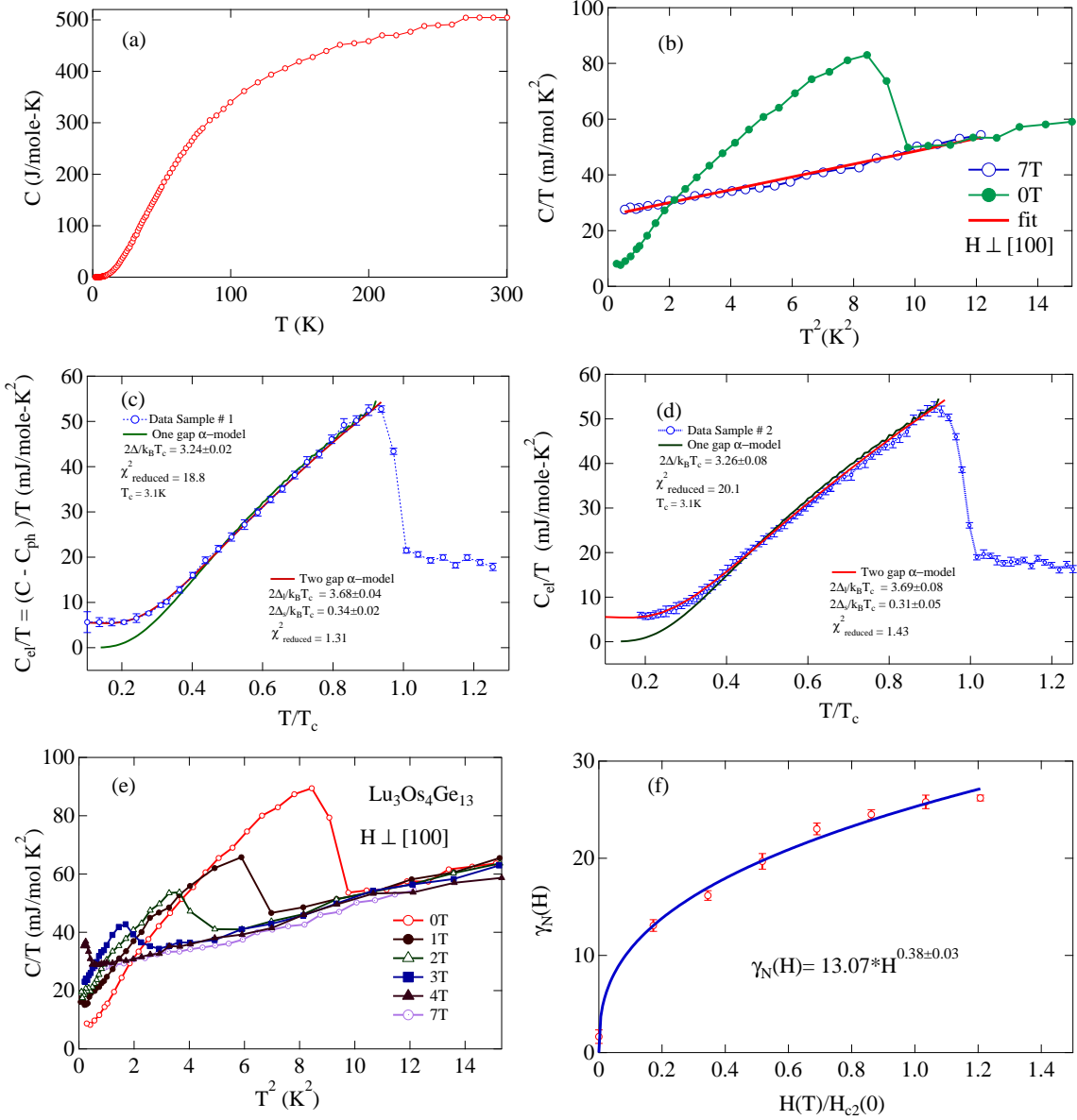


FIG. 3. (Color online) (a) Specific heat capacity (C) vs temperature of $\text{Lu}_3\text{Os}_4\text{Ge}_{13}$ from 1.8-300 K. (b) Normal state heat capacity data taken at 7T fitted to the equation $C(T) = \gamma_N T + \beta T^3$. The zero field data shows sharp jump at 3.1K. (c) Low temperature electronic heat capacity data for sample #1 fitted using: (i) one-gap α -model (anisotropic gap) and (ii) Two-gap α -model for a multi-band BCS superconductor. (d) Low temperature electronic heat capacity data for sample #2 fitted using: (i) one-gap α -model (anisotropic gap) and (ii) Two-gap α -model for a multi-band BCS superconductor. (e) The heat capacity in the mixed state in different magnetic fields. The linear extrapolations at $T=0$ of the low temperature heat capacity data at different fields are used to estimate the values of Sommerfeld coefficient $\gamma_N(H)$ in the superconducting state. (f) The magnetic field dependence of $\gamma_N(H)$.

$25.4 \pm 0.3 \frac{\text{mJ}}{\text{mol K}^2}$ and the phonon/lattice contribution coefficient $\beta = 2.30 \pm 0.05 \frac{\text{mJ}}{\text{mol K}^4}$ from the fit. The Debye temperature (Θ_D), calculated using the formula,

$$\Theta_D = (12\pi^4 R N / 5\beta)^{\frac{1}{3}}, \quad (8)$$

where R is the molar gas constant and $N(= 20)$ is the number of atoms per formula unit (f.u.), is 256.6 ± 0.7 K. The density of states at the Fermi level calculated using the formula $\gamma_n = (\pi^2 k_B^2 / 3) D(E_F)$, is $D(E_F) = 21.3$ states/eV-f.u. for both spin directions. This density of state contains quasiparticle mass enhancement by many-body electron-phonon interaction and is related to bare density of states $D_{band}(E_F)$ by $D(E_F) = (1 + \lambda_{\text{eph}}) D_{band}(E_F)$,

where λ_{eph} is the dimensionless electron-phonon coupling constant. λ_{eph} is related to the phonon spectrum and density of states in Eliashberg theory¹³ and represents the strength of electron-phonon coupling. λ_{eph} can be calculated using McMillan's formula¹⁴,

$$\lambda_{\text{eph}} = \frac{1.04 + \mu^* \ln(\Theta_{\text{D}}/1.45T_c)}{(1 - 0.62\mu^*) \ln(\Theta_{\text{D}}/1.45T_c) - 1.04}, \quad (9)$$

where μ^* is the repulsive screened coulomb parameter. The competition between μ^* and λ_{eph} is the determining factor for Cooper pairing in conventional superconductors¹⁵. The value of μ^* is taken as 0.13. Using equation (9), we obtain $\lambda_{\text{eph}} = 0.58$. This suggests a moderately enhanced electron-phonon coupling in $\text{Lu}_3\text{Os}_4\text{Ge}_{13}$. Combining the values of λ_{eph} and $D(E_F)$, we get $D_{\text{band}}(E_F) = 13.48$ states/eV-f.u. for both spin directions. The effective mass of the quasiparticles (m^*), calculated using the relation, $m^* = (1 + \lambda_{\text{eph}})m_{\text{band}}$ is $m^* = 1.58m_e$, assuming effective band mass $m_{\text{band}} = m_e$, the free electron mass.

The sharp jump in the electronic heat capacity $\Delta C_{el}(T)$ at T_c , is 89.6 mJ/mol K, giving the ratio $\Delta C_{el}/\gamma_n T_c = 1.15$. This ratio can be used to understand the strength of the electron-phonon coupling. This ratio is smaller than the weak-coupling limit value of 1.43 for a conventional BCS superconductor. If we consider a single band model¹⁶ for a BCS superconductor, such a reduction in the heat capacity jump can be either due to the presence of anisotropic superconducting energy gap or presence of multiple gaps at the Fermi surface in the superconducting state.

Apart from the reduced jump in the heat capacity at T_c , the low temperature electronic heat capacity is higher than the expected value for a single gap s-wave BCS superconductor (see Fig. 3(c) and (d)). To analyze the suppression in the heat capacity jump and the low temperature data in more detail, we have used empirical (and not self-consistent) one-band one-gap α -model (which accounts for anisotropy in the order parameter Δ_0 at the Fermi surface) and two-band two-gap α -model^{16,22}. In these models, the superconducting energy gap ($\Delta(t)$) is parametrised in terms of normalised BCS gap ($\delta(t)$), $\Delta(t) = \Delta_0 \delta(t)$, where $t (= T/T_c)$ is the reduced temperature. The normalised BCS gap as a function of reduced temperature is taken from the Muhlschlegel's paper²⁹. The entropy (S) and the heat capacity (C) for a system of independent fermionic-quasiparticles can be written as,

$$\frac{S}{\gamma_n T_c} = -\frac{6}{\pi^2} \frac{\Delta_0}{k_B T_c} \int_0^\infty [f \ln f + (1-f) \ln(1-f)] dy, \quad (10)$$

$$\frac{C_{el}}{\gamma_n T_c} = t \frac{d(S/\gamma_n T_c)}{dt}, \quad (11)$$

where $f = [e^{\beta E} + 1]^{-1}$, $\beta = (k_B T)^{-1}$ and $y = \varepsilon/\Delta_0$. The quasiparticle energy (E) is $\sqrt{\varepsilon^2 + \Delta^2(t)}$, where ε is the energy of the normal electrons measured from the Fermi level. Using equation (10) and (11), we can write the electronic heat capacity for one-gap α -model as,

$$C_{el}(a, \alpha, t) = a \int_0^\infty \left[\left(\frac{x}{t} \right)^2 + \alpha^2 \left(\frac{\delta(t)}{t} \right)^2 - \alpha^2 \left(\frac{\delta(t)}{t} \right) \left(\frac{d\delta(t)}{dt} \right) \right] \text{sech}^2 \left(\sqrt{\left(\frac{x}{t} \right)^2 + \alpha^2 \left(\frac{\delta(t)}{t} \right)^2} \right) dx, \quad (12)$$

where $a = 12\gamma_n T_c/\pi^2$, $x = \varepsilon/2k_B T_c$ and $\alpha = \Delta/2k_B T_c$. In the two-gap model, the total electronic heat capacity, $C_{tot}(a_1, \alpha_1, a_2, \alpha_2, t)$, is taken as the sum of the independent contributions from two-bands with different superconducting energy gaps, each following BCS type temperature dependence (if we neglect inter-band transitions due to scattering by impurities or phonons, and assume that $\gamma_{n,l} + \gamma_{n,s} = \gamma_n$). For the two-gap α -model, the total heat capacity is given by,

$$C_{tot}(a_1, \alpha_1, a_2, \alpha_2, t) = C_{el}(a_1, \alpha_1, t) + C_{el}(a_2, \alpha_2, t), \quad (13)$$

where $a_1 = 12\gamma_{n,l} T_c/\pi^2$, $\alpha_1 = \Delta_l/2k_B T_c$, $a_2 = 12\gamma_{n,s} T_c/\pi^2$ and $\alpha_2 = \Delta_s/2k_B T_c$. The subscripts 'l' and 's' stand for large and smaller gap respectively.

We estimate the fitting parameters (a, α for the one-gap α -model; and $a_1, \alpha_1, a_2, \alpha_2$ for two-gap α -model) using nonlinear least-squares fit for two different samples in order to confirm the reproducibility of the results. To estimate the uncertainties in the fitted parameters, we repeat the whole process for 1000 realizations of the data obtained by adding random perturbations to the data with the standard deviation equal to 1σ uncertainty in the corresponding data point for both samples. The median value of each parameter for 1000 realizations was accepted as the fitted value, while the $\pm 1\sigma$ uncertainty in the fitted value was estimated from the range covering 34% of the area on either side of the median in the distribution function of the fitted parameter. Fig. 3(c) and fig. 3(d) show the fit to the electronic specific heat for the two samples using one-gap α -model and two-gap α -model. The one-gap α -model fails to fit the data at

the low temperatures with large values of chi-square per degree of freedom ($\chi_{\text{pdf}}^2 = 18.8$ and 20.1 for sample #1 and sample #2 respectively). The low temperature electronic heat capacity of both samples is best described by the two-gap α -model with $\chi_{\text{pdf}}^2 = 1.31(1.43)$. Clearly, the two-gap α -model fits the data significantly better than the one-gap α -model. We find the two gaps to be $2\Delta_l/k_B T_c = 3.68 \pm 0.04$ (3.69 ± 0.08) and $2\Delta_s/k_B T_c = 0.34 \pm 0.02$ (0.31 ± 0.05) for sample # 1 (sample # 2). The contributions of $\gamma_{n,l}$ and $\gamma_{n,s}$ to γ_n are 81.5% and 18.5% respectively.

The study of vortex excitations in the mixed state provides insight in the understanding of the superconducting order parameter. Fig. 3(e) shows the low temperature electronic heat capacity in different magnetic fields ($H_{c1} < H < H_{c2}$). The linear extrapolations to zero temperature give the heat capacity contribution due to normal electrons in the mixed state, and are determined in terms of the electronic specific heat coefficient $\gamma_N(H)$. This electronic contribution is attributed to the normal state electrons present in the vortex cores. In s-wave superconductors, the vortex cores contribute to the electronic heat capacity as normal metals. This contribution is proportional to the number of vortices and hence proportional to the applied magnetic field, i.e. $\gamma_N(H) \propto H$. However, we find that $\gamma_N(H) = 13.07H^{0.38 \pm 0.03}$ as shown in the Fig. 3(f). A nonlinear dependence of $\gamma_N(H)$ on the magnetic field has been argued to be intrinsic property of the multi-band, multi-gap superconductors²⁵. This analysis also suggests the presence of multiple gaps at the Fermi level in the superconducting state and indicate multi-band superconductivity in $\text{Lu}_3\text{Os}_4\text{Ge}_{13}$ single crystal.

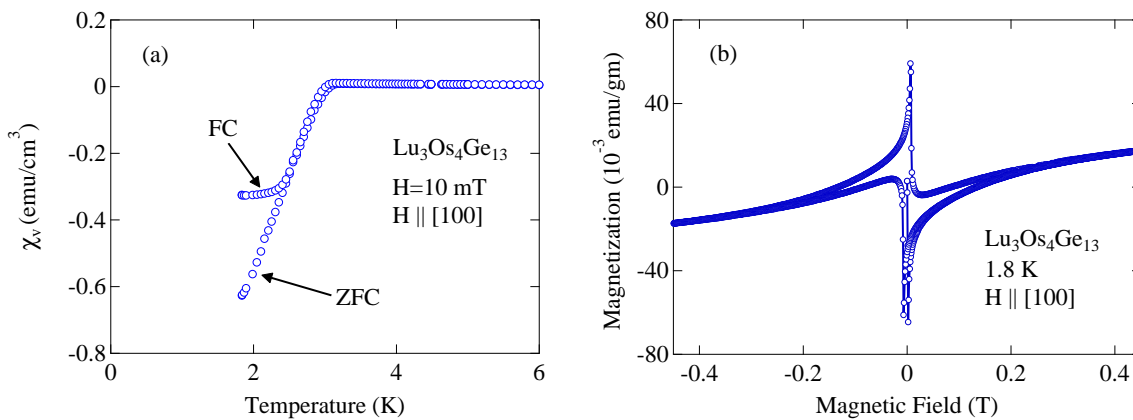


FIG. 4. (Color online) (a) DC magnetic susceptibility data as function of temperature. The superconducting transition temperature, as determined from susceptibility measurement is in excellent agreement with the resistivity data. The ZFC and FC susceptibility data indicate significant amount of pinning of vortices in the compound. (b) Magnetization as a function of magnetic field for $H \parallel [100]$ direction. The M-H loop is closed ($\delta M = 0$) at magnetic fields $H \geq 0.45 T$ at 1.8 K, which suggests possible melting of vortices at 0.45 T field.

Fig. 4(a) shows a diamagnetic transition into superconducting state at 3.1 K in the low temperature dc-susceptibility data. Significant amount of vortex pinning can be observed by comparing the zero field cooled (ZFC) and the field cooled (FC-Meissner) data below the transition temperature. The sample is weakly paramagnetic at room temperature ($\chi = 3 \times 10^{-4}$ emu/mole at $T=300\text{K}$). The temperature dependence of the susceptibility is Pauli paramagnetic type with small rise at low temperature ($\chi = 8 \times 10^{-3}$ emu/mole at $T=3.2\text{K}$) possibly due to the presence of small magnetic rare-earth impurities (ppm level) in Lu. We estimate the value of the lower critical field $H_{c1}(1.8\text{K}) = 20$ mT from magnetization measurements. The value of the lower critical field $H_{c1}(0) = 30$ mT is obtained using the following expression,

$$H_{c1}(0) = H_{c1}(T)/(1 - (T/T_c)^2). \quad (14)$$

Substituting the values of $\xi_{GL}(0)$ and $H_{c1}(0)$ in the following expression,

$$H_{c1}(0) = \frac{\Phi_0}{4\pi\lambda_{GL}^2} \ln\left(\frac{\lambda_{GL}}{\xi_{GL}}\right), \quad (15)$$

we obtain $\lambda_{GL}(0) = 4736 \text{ \AA}$. The Ginzburg-Landau parameter $\kappa_{GL}(0) = \frac{\lambda_{GL}(0)}{\xi_{GL}(0)} = 61$. Using the formula,

$$H_{c1}(0) = \frac{H_c(0)}{\sqrt{2}\kappa} (\ln \kappa + 0.5), \quad (16)$$

we obtain the value of the thermodynamic critical field $H_c(0) = 564 \text{ mT}$. The magnetization (M-H) data as shown in Fig. 4(b) shows that the M-H loop is closing at magnetic fields $H > 0.45 \text{ T}$ at 1.8 K, suggesting the unpinning (melting) of vortices in magnetic fields much smaller than the of upper critical field ($\mu_0 H_{c2}(1.8 \text{ K}) = 3.2 \text{ T}$). An unpinned vortex phase exists in the magnetic field region $0.45 \text{ T} \leq H \leq \mu_0 H_{c2}(1.8 \text{ K}) = 3.2 \text{ T}$, which may be a vortex liquid phase. Similar vortex liquid phase is observed in high T_c superconductors¹⁰ and is an unusual phenomena in low T_c superconductors. Though the melting of the vortices in high T_c superconductors is attributed to quantum and thermal fluctuations^{10,17}, there is no clear understanding of the origin of vortex liquid phase in low T_c superconductors. The strength of the thermal fluctuations, which leads to the vortex unpinning, is described in terms of the Ginzburg number given by,

$$G_i = \frac{1}{2} \left(\frac{k_B \mu_0 \Gamma T_c}{4\pi \xi^3(0) H_c^2(0)} \right)^2, \quad (17)$$

where Γ is the anisotropy parameter (≈ 1 for cubic $\text{Lu}_3\text{Os}_4\text{Ge}_{13}$). Using equation (17), we get the value of the Ginzburg number $G_i = 4.1 \times 10^{-6}$. The value of Ginzburg number for $\text{Lu}_3\text{Os}_4\text{Ge}_{13}$ is larger than low T_c superconductors ($\approx 10^{-8}$) but smaller than high T_c superconductors ($\approx 10^{-2}$)^{10,17}. This suggests that the thermal fluctuations, though weak, may play an important role in the unpinning of the vortices in this compound.

Type-II superconductors in which H_{c1} and H_{c2} are well separated ($H_{c2}/H_{c1} \sim \kappa^2$) are classified as strongly type-II superconductors. This ($H_{c1} \ll H_{c2}$) leads to a situation in which the magnetic fields associated with vortices overlap and the superposition becomes nearly homogeneous, while the order parameter characterizing superconductivity is still inhomogeneous¹⁷. Detailed penetration depth (λ_{GL}) measurements are required to obtain correct values of H_{c1} and κ .

The analysis of the electronic band structure and density of states of $\text{Lu}_3\text{Os}_4\text{Ge}_{13}$, based on the electronic structure calculations using Wien2K, is presented below. The left panel in Fig. 5 shows the band structure of $\text{Lu}_3\text{Os}_4\text{Ge}_{13}$ near the Fermi level. The band structure has multi-valley type character⁸. Three bands cross the Fermi level and account for metallic nature of the compound. The right panel in Fig. 5 shows the calculated density of states (DOS) for one formula unit (20 atoms) of $\text{Lu}_3\text{Os}_4\text{Ge}_{13}$.

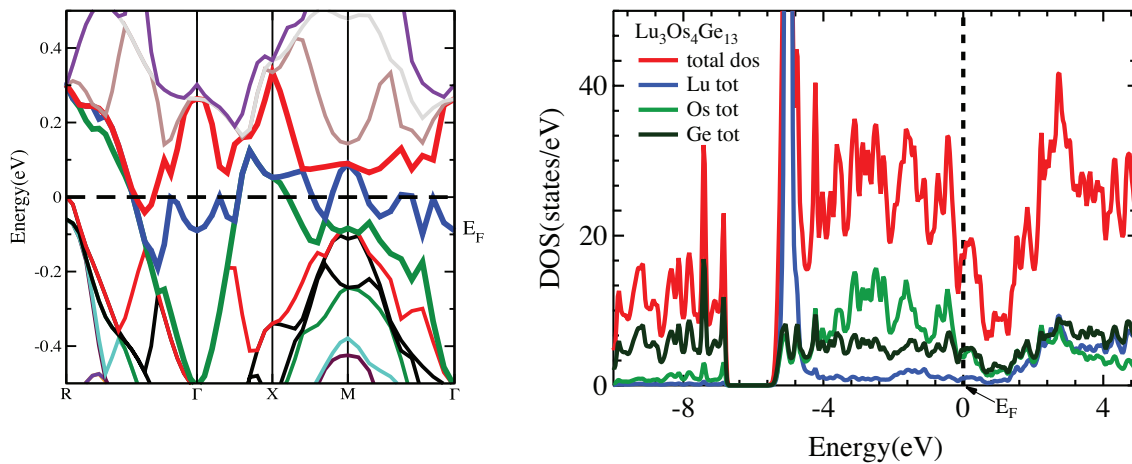


FIG. 5. (Color online) (*Left panel*) Band structure of $\text{Lu}_3\text{Os}_4\text{Ge}_{13}$ near Fermi level. The band structure shows a multi-valley type character. Three bands shown in bold lines cross the Fermi-surface. (*Right panel*) Analysis of density of states of $\text{Lu}_3\text{Os}_4\text{Ge}_{13}$. The total DOS curve has a local maximum at the edge of the Fermi energy. The partial density of states curves show that the major contribution to the total density of states is coming from Os and Ge atoms. Lu atoms have least contribution to the total density of states.

The Fermi level is located near the edge of a local maxima in total density of states. The value of the DOS at E_F is $\approx 17 \text{ states/eV-f.u}$ for both spin directions. This value is smaller than the value ($\approx 21 \text{ states/eV-f.u}$ for both spin directions) calculated using the value of γ_n obtained from heat capacity measurements, which indicates the mass-enhancement in the compound, since no electronic correlations were taken into account in the band structure calculations. The partial DOS shows that the total DOS is dominated by contributions from Os and Ge. Fig. (6) shows the calculated Fermi surfaces for the three bands (as well as all the bands plotted together) which cross the Fermi level. The combination of these bands leads to a complex Fermi surface (Fig. 6).

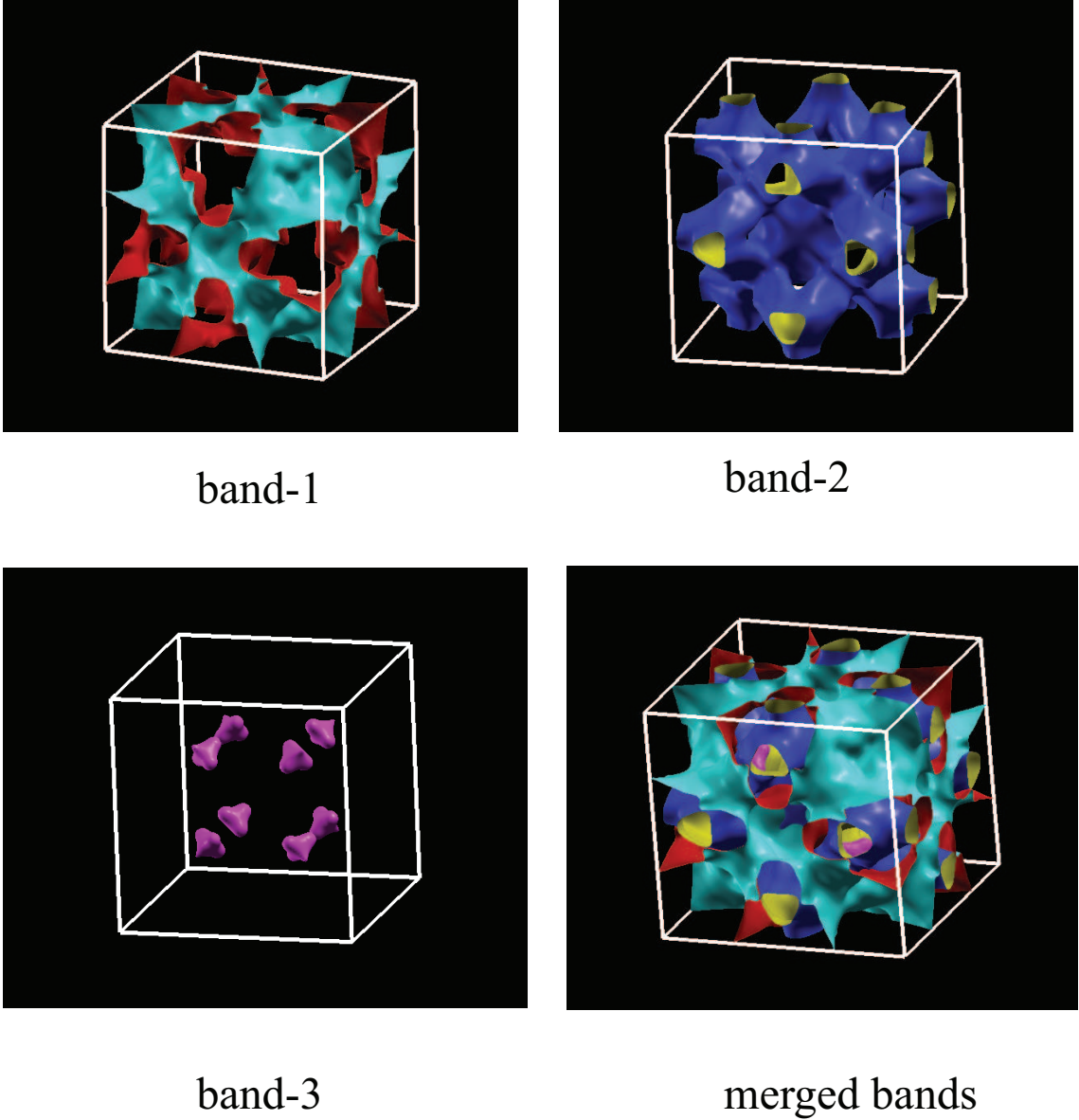


FIG. 6. (Color online) Contributions of the bands crossing the Fermi level to the Fermi surface. All the three bands are plotted together make a complex surface.

IV. CONCLUSION

In summary, we have studied the superconducting properties of $\text{Lu}_3\text{Os}_4\text{Ge}_{13}$ in detail using electrical transport, magnetization and heat capacity measurements. We show that $\text{Lu}_3\text{Os}_4\text{Ge}_{13}$ is multi-band type-II superconductor ($T_c = 3.1\text{K}$) by analyzing the low temperature heat capacity data using empirical two-gap multi-band α -model. The single band WHH model does not fully explain the temperature dependence of the upper critical field $H_{c2}(T)$, suggesting presence of multi-band effects in $\text{Lu}_3\text{Os}_4\text{Ge}_{13}$. The analysis of the low temperature heat capacity data for two different samples of $\text{Lu}_3\text{Os}_4\text{Ge}_{13}$ single crystal using two-gap α -model confirms the presence of two superconducting gaps ($2\Delta_l/k_B T_c = 3.68 \pm 0.04(3.69 \pm 0.08)$ and $2\Delta_s/k_B T_c = 0.34 \pm 0.02(0.31 \pm 0.05)$) in the compound. The magnetization measurements show a large reversible region in the mixed state, similar to the vortex liquid phase observed in high- T_c superconductors. The estimation of the Ginzburg number G_i suggests that thermal fluctuations (though small) may play an important role in the unpinning of the vortices in this compound. Electronic band structure calculations along with heat capacity measurements suggest that the electronic correlations are not significant in $\text{Lu}_3\text{Os}_4\text{Ge}_{13}$. Band structure calculations show a very complex structure in the fermi surface which might play

significant role in enhancing multi-band effects in $\text{Lu}_3\text{Os}_4\text{Ge}_{13}$.

V. ACKNOWLEDGMENTS

We thank Dr. Susanta K. Mohanta, Prof. Surendra Nath Mishra, Dept. of Nuclear & Atomic Physics, Dr. Sutirtha Mukhopadhyay, Prof. Pratap Raychaudhuri, Dept. of Condensed Matter Physics & Material Science and Kuldeep Verma, Dept. of Astronomy and Astrophysics, TIFR for useful discussions.

VI. REFERENCES

-
- * Om Prakashop1111shukla@gmail.com
- ¹ Slebarski, A. et. al. Superconductivity of $\text{La}_3\text{Co}_4\text{Sn}_{13}$ and $\text{La}_3\text{Rh}_4\text{Sn}_{13}$: A comparative study, *Phys. Rev. B* **89**, 125111; DOI:10.1103/PhysRevB.89.125111 (2014).
 - ² Remeika, J. P. et al. A new family of intermetallic superconducting/magnetic stannides, *Solid State Commun.* **34**, 923; DOI:http://dx.doi.org/10.1016/0038-1098(80)91099-6 (1980).
 - ³ Segre, C. U. et al. Ternary superconductors of the $\text{Sc}_5\text{Co}_4\text{Si}_{10}$ type, *Ternary Superconductors*, **34**, 243; DOI:http://dx.doi.org/10.1016/0038-1098(80)91099-6 (1981).
 - ⁴ Ramakrishnan, S. et. al. Absence of bulk magnetic ordering in $\text{Pr}_3\text{Ru}_4\text{Ge}_{13}$, *Journal of Magnetism and Magnetic Materials*, **152**, 375; DOI: http://dx.doi.org/10.1016/0304-8853(95)00471-8 (1996).
 - ⁵ Ghosh, K. et. al. Crystal structures and low-temperature behaviors of the heavy-fermion compounds CeRuGe_3 and $\text{Ce}_3\text{Ru}_4\text{Ge}_{13}$ containing both trivalent and tetravalent cerium, *Phys. Rev. B* **52**, 7267; DOI:10.1103/PhysRevB.52.7267 (1995).
 - ⁶ Ghosh, K. et al. Resistivity and magnetic-susceptibility studies in the $\text{R}_3\text{Ru}_4\text{Ge}_{13}$ (R=Nd, Dy, Ho, Er, Yb, Lu, and Y) system, *Phys. Rev. B* **48**, 10435; DOI:10.1103/PhysRevB.48.10435 (1993).
 - ⁷ Kong, H. et al. Thermoelectric properties of rare earth-ruthenium-germanium compounds, *J. Appl. Phys.* **102**, 023702; DOI:http://dx.doi.org/10.1063/1.2753592 (2007).
 - ⁸ Cohen, Marvin L. Superconductivity in Many-Valley Semiconductors and in Semimetals, *Phys. Rev.* **134**, A511A521; DOI:10.1103/PhysRev.134.A511 (1964).
 - ⁹ Helfand, E. and Werthamer, N. R. Temperature and Purity Dependence of the Superconducting Critical Field, H_{c2} . II, *Phys. Rev.* **147**, 1; DOI:http://dx.doi.org/10.1103/PhysRev.147.288 (1966).
 - ¹⁰ Blatter, G. et. al. Vortices in high-temperature superconductors, *Rev. Mod. Phys.* **66**, 1125; DOI:10.1103/RevModPhys.66.1125 (1994).
 - ¹¹ Werthamer, N. R et al. Temperature and Purity Dependence of the Superconducting Critical Field, H_{c2} . III. Electron Spin and Spin-Orbit Effects, *Phys. Rev.* **147**, 295; DOI:10.1103/PhysRev.147.295 (1966).
 - ¹² Maki, Kazumi Effect of Pauli Paramagnetism on Magnetic Properties of High-Field Superconductors, *Phys. Rev.* **148**, 362; DOI:10.1103/PhysRev.148.362 (1966).
 - ¹³ Eliashberg, G.M. Interaction between electrons and lattice vibrations in a superconductors, *Soviet Physics (JETP)* **11**, 3 (1960).
 - ¹⁴ McMillan, W. L. Transition Temperature of Strong-Coupled Superconductors, *Phys. Rev.* **167**, 331; DOI:10.1103/PhysRev.167.331 (1968).
 - ¹⁵ Bardeen, J. et al. Theory of Superconductivity, *Phys. Rev.* **108**, 1175; DOI:10.1103/PhysRev.108.1175 (1957).
 - ¹⁶ Padamsee, H. et al. Quasiparticle phenomenology for thermodynamics of strong-coupling superconductors, *Journal of Low Temperature Physics* **12**, 387; DOI:10.1007/BF00654872 (1973).
 - ¹⁷ Rosenstein, Baruch et al. Ginzburg-Landau theory of type II superconductors in magnetic field, *Rev. Mod. Phys.* **82**, 109; DOI:10.1103/RevModPhys.82.109 (2010).
 - ¹⁸ Prakash, Om et al. Superconductivity in a low carrier density system: A single crystal study of cubic $\text{Y}_3\text{Ru}_4\text{Ge}_{13}$, *Physica C: Superconductivity*, **492**, 90; DOI:http://dx.doi.org/10.1016/j.physc.2013.05.014 (2013).
 - ¹⁹ Rodriguez-Carvajal, J. Recent advances in magnetic structure determination by neutron powder diffraction, *Physica B* **192**, 55; DOI:http://dx.doi.org/10.1016/0921-4526(93)90108-1 (1993).
 - ²⁰ Blaha, P. et.al. WIEN2k, An Aug- mented Plane Wave + Local Orbitals Program for Calculating Crystal Properties (Karlheinz Schwarz, Techn. Universitat Wien, Austria), 2001. ISBN 3-9501031-1-2.
 - ²¹ Madsen, Georg K. H. et.al. Efficient linearization of the augmented plane-wave method, *Phys. Rev. B* **64**, 195134; DOI:10.1103/PhysRevB.64.195134 (2001).
 - ²² Kogan, V. G. and Martin, C. and Prozorov, R. et.al. Superfluid density and specific heat within a self-consistent scheme for a two-band superconductor, *Phys. Rev. B* **80**, 014507; DOI:10.1103/PhysRevB.80.014507.

- ²³ Perdew, John P. *et al.* Generalized Gradient Approximation Made Simple, *Phys. Rev. Lett.* **77**, 3865; DOI:10.1103/PhysRevLett.77.3865 (1996).
- ²⁴ Volovik, G. E. Superconductivity with lines of gap nodes: density of states in the vortex, *JETP Lett.* **58**, 469 (1993).
- ²⁵ Yang, H.D. *et al.* Order Parameter of MgB₂: A Fully Gapped Superconductor, *Phys. Rev. Lett.* **87**, 167003; DOI:10.1103/PhysRevLett.87.167003 (2001).
- ²⁶ Clogston, A. M.*et al.* Upper Limit for the Critical Field in Hard Superconductors, *Phys. Rev. Lett.* **9**, 266; <http://dx.doi.org/10.1103/PhysRevLett.9.266>.
- ²⁷ Gurevich, A.*et al.* Upper critical field and the Fulde-Ferrel-Larkin-Ovchinnikov transition in multiband superconductors, *Phys. Rev. B.* **82**, 184504; DOI:10.1103/PhysRevB.82.184504.
- ²⁸ Chandrasekhar, B. S. *et al.* A note on the maximum critical field of high-field superconductors, *Applied Physics Letters* **1**, 7-8 ; DOI:<http://dx.doi.org/10.1063/1.1777362> .
- ²⁹ Muhlshlegel B. Die thermodynamischen funktionen des supraleiters, *Z. Phys.*, **155**, 313 (1959).
- ³⁰ Shi, X. and Zhang, W. and Chen, L. D. and Yang, J. and Uher, C. *et al.* Theoretical study of the filling fraction limits for impurities in CoSb₃, *Phys. Rev. B* **75**, 235208; DOI:10.1103/PhysRevB.75.235208 .